

Image-based plant disease diagnosis with unsupervised anomaly detection based on reconstructability of colors

Ryoya Katafuchi ¹*, *Terumasa Tokunaga¹*,

1 Department of Systems Design and Informatics, Kyushu Institute of Technology, Iizuka, Fukuoka, JAPAN

✉

* tokunaga@ces.kyutech.ac.jp

Abstract

This paper proposes an unsupervised anomaly detection technique for image-based plant disease diagnosis. A construction of large and openly available data set on labeled images of *healthy* and *diseased* crop plants has led to growing interest in computer vision techniques for plant disease diagnosis. Although supervised image classifiers based on deep learning could be a powerful tool to identify plant diseases, they require huge amount of data set that have been labeled as *healthy* and *disease*. While, data mining techniques called anomaly detection includes unsupervised approaches that not require rare samples for training classifiers. The proposed method in this study focuses on the reconstructability of colors on plant images. We expect that a deep encoder decoder network trained for reconstructing colors of *healthy* plant images fails to color symptomatic regions. The main contributions of this work are as follows: (i) we propose a new image-based plant disease detection framework utilising a conditional adversarial network called pix2pix, (ii) we introduce a new anomaly score calculated from CIEDE2000 color difference. Through experiments using the PlantVillage dataset, we demonstrate that our method is superior to an existing anomaly detector called AnoGAN for identifying diseased crop images in terms of accuracy, interpretability and computational efficiency.

Introduction

Diagnosis of plant diseases is an important task for food safety and security. To develop accurate image classifiers for plant disease diagnosis, the PlantVillage project [1] was started. It provides thousands of labeled images of healthy and diseased crop plants collected under controlled conditions. Using the large and publicly available datasets, some challenges based on deep learning have been made to establishing an accurate image classifier for plant disease diagnosis.

Some challenges based on deep convolution neural networks have been met pursuant of establishing an accurate image classifier using PlantVillage dataset. With a comprehensive experiment using color crop images, AlexNet and GoogleNet achieved an average accuracy of over 90% on a held-out test set for identifying 26 diseases in 14 crop species [2]. Similarly, it was reported that LeNet showed an effective performance in a classification test of banana leaves diseases under challenging severe conditions [3]. Ferentinos (2018) [4] compared performances of five CNN models using leaf images obtained in both laboratory conditions and real conditions. The result showed that a VGG convolutional neural network achieved the highest performance with a success rate of 99.53%. Another comparison study using PlantVillage dataset showed an outstanding performance of Deep Learning in comparison with conventional machine learning techniques [5].

A series of the previous researches warrant further developments of image-based plant disease diagnosis techniques for more practical . Supervised image classifiers based on deep learning require huge amount of data set that have been labeled as *healthy* and *disease* for training a classifier. A correction of samples with rare diseases often imposes higher burden on human annotators, which could be a severe bottleneck in practical applications To improve that,it is required further studies for developing an image-based plant disease diagnosis technique that is free from annotation costs for rare samples.

Anomaly detection is a data mining technique for identifying irregular or unusual patterns in datasets. These techniques are significant for a wide range of applications such as fraud detection for financial services, intrusion detection for networks, identification of disease markers for medical diagnosis and failure detection for engineering systems. Typical approaches to anomaly detection are based on conventional machine learning techniques. For unlabelled data, simple clustering approaches are used [6] [7]. For cases where normal and anomalous labels are available, simple classification approaches such as support vector machines are used [8].

Recently, in the field of machine learning and computer vision, many anomaly detection techniques based on a deep neural network have been proposed. Such *deep* anomaly detection approaches can be roughly categorized into three groups based on the type of machine learning, that is, supervised approaches [9], unsupervised approaches [10], [11], [12], [13], [14], [15] and semi-supervised approaches [16], [17], [18] (see [19] for a comprehensive survey).

Generative adversarial networks (GANs) [20] have had a great deal of success with image generation tasks [21] [22] [23] [24] [25] [26]. The excellent expressive power of GANs has led to growing interest in utilizing these networks for real-world data analysis including anomaly detection. Typical approaches with GANs are based on the idea of adversarial feature learning [27] on normal data and the measurement of anomaly scores for a given query image. AnoGAN [28] is the first approach that realizes the concept. It provides an unsupervised way of detecting real-world anomalies including the discovery of novel anomalies in medical imaging data. Recently, some extensions of AnoGAN were proposed to overcome performance issues [29] [30] or to improve computational efficiency [31].

AnoGAN computes the anomaly score based on the reconstructability of normal samples. Since AnoGAN does not require anomalous data for training neural networks, it can be applicable for diverse problems including those within the natural sciences. However, this approach can be criticized because it does not explicitly pay attention to colors in imaging data. In many real-world problems, color information is essential to discovering anomalies in datasets. For example, discoloration observed on leaves can be crucial information for detecting symptoms [32].

To the best of the authors' knowledge, there are no extensions of AnoGAN that focus on detecting anomalies dominantly appearing in colors. Moreover, AnoGAN has two drawbacks for real time applications. One is that AnoGAN requires huge normal data sufficient to learn a manifold of normal variability. In addition to this, it requires an iterative procedure for calculating anomaly scores, which reduces computational efficiency.

In this paper, we propose a new anomaly detection method intended to detect diseases in plants at an image level and visualize symptomatic regions at a pixel level. Our approach uses a conditional adversarial network called pix2pix [26] for learning inverse mapping from converted grayscale images to original color images. Since the strategy is simple, it can be expected to work well even in cases where we do not have a large dataset of normal instances, which unlike to AnoGAN. To explore the utility of the proposed method, we use the PlantVillage dataset. This is a publicly available image dataset for developing automatic diagnostic techniques to identify plant diseases. Additionally, we propose a simple, easy-to-interpret anomaly score that is based on CIEDE2000 color difference. Since our method does not require any iterative procedure for calculating anomaly score, the level of computational efficiency is expected to be practical for real time disease detection.

Related Work

As we mentioned, the present work is motivated by AnoGAN [28] and its extensions [29] [30] [31]. The fundamental idea of AnoGAN relies on a reconstruction of normal data from latent variables. The framework can be applicable for diverse problems, but its effectiveness for detecting anomalies strongly appearing in color has not been demonstrated in previous studies. On the other hand, our approach relies on a reconstruction of colors. Specifically, we suppose that a rich generative model trained for reconstructing colors of normal data fails to color anomalous regions in images. Unlike AnoGAN and its extensions, our interest herein is focused on the detection of color anomalies such as discolored parts on plants. Thus the proposed method can be viewed as an extension of AnoGAN in a different direction from previous studies.

Method

Outline of the proposed method

Fig. 1 is a schematic view of the proposed method. It consists of five processing steps for image-level detection and pixel-level visualization of plant diseases.

1. **Preparing:** Our method detects anomalies in color images in terms of the reconstructability of colors at the pixel level using a conditional adversarial network. Consider a set of M pairs of color images and grayscale images. Let $\mathbf{I}_c(x_i) \in \mathbb{R}_+^3$ ($i = 1, 2, \dots, 256 \times 256$) be a pixel value representing a color on the pixel position x_i . Similarly, let $I_g(x_i) \in \mathbb{R}_+$ ($i = 1, 2, \dots, 256 \times 256$) be a pixel value representing an intensity on the pixel position x_i . Also, for notational simplicity, we express a color image and a grayscale image as \mathbf{I}_c and \mathbf{I}_g , respectively. We use these pairs of images, \mathbf{I}_c and \mathbf{I}_g , for training GANs in such a way that the DCED network learns an inverse mapping $G : \mathbf{I}_g \mapsto \mathbf{I}_c$. We note that these training images are selected only from normal data. While, test data includes both normal and anomalous data. For evaluation purposes, we use a set of N color images with an array of binary image-wise ground-truth labels $l_n \in \{1, -1\}$ ($n = 1, 2, \dots, N$).
2. **Training:** The left half of Fig. 1 illustrates concurrent training on generator and discriminator networks. Pairs of images \mathbf{I}_g and \mathbf{I}_c are used as the input and output of G , respectively. Also, pairs of \mathbf{I}_c and $G(\mathbf{I}_g)$ are used as *fake* pairs for training the discriminator network D .
3. **color reconstruction:** For test data, we obtain a reconstructed color image, denoted by $\hat{\mathbf{I}}'_c$, from a query color image \mathbf{I}'_c by using the trained generator network.
4. **Calculation of color anomaly score:** We calculate an anomaly score for a given query color image $\tilde{\mathbf{I}}_c$ based on color differences between the reconstructed color image $G(\mathbf{I}'_c)$ and the original color image \mathbf{I}'_c . The color difference d_i is calculated from $\mathbf{I}'_c(x_i)$ and $\hat{\mathbf{I}}'_c(x_i)$ for all i . The anomaly score based on color difference is obtained by simply summing d_i for all i .
5. **Anomaly detection:** Finally, a query image is classified into normal or anomalous data by a simple thresholding of the anomaly score.

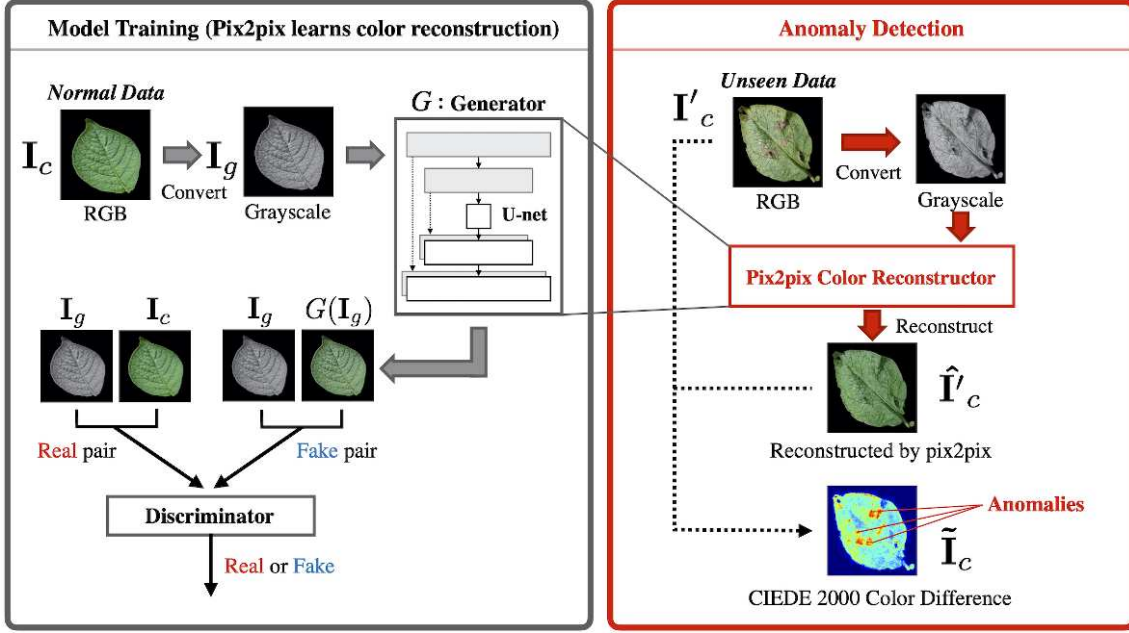


Fig 1. Outline of the proposed method.

color reconstruction by Pix2pix

We use pix2pix [26] for color reconstruction. Pix2pix is a general framework for image-to-image translation based on deep convolutional GANs (DCGANs). The generator network in pix2pix is U-Net, which is a DCED network with skip structures. It is well-known that skip structures enable a DCED network to learn both global and local features efficiently. The discriminator in pix2pix is the convolutional PatchGAN, which only penalizes structure at the patch scale.

Here let the input and output variable for pix2pix be x and y , respectively. Now the loss function for training pix2pix can be expressed as follows:

$$L_{cGAN}(G, D) = \mathbb{E}_{x,y}[\log D(x, y)] + \mathbb{E}_{x,z}[\log (1 - D(x, G(x, z)))] \quad (1)$$

where $\mathbb{E}[\cdot]$ indicates the expected value and z is a random noise vector. During training, pix2pix seeks to minimise L_{cGAN} with respect to G , and at the same time maximise it with respect to D under L_1 -regularization:

$$\begin{aligned} G* &= \arg \min_G \max_D \mathbb{E}_{x,y}[\log D(x, y)] + \mathbb{E}_{x,z}[\log (1 - D(x, G(x, z)))] \\ &+ \lambda \mathbb{E}_{x,y,z}[\|y - G(x, z)\|_1] \end{aligned} \quad (2)$$

where $\|\cdot\|_1$ indicates the L_1 -norm and λ is a hyperparameter which controls the strength of the regularization term (see [26] for more details).

CIEDE2000 color anomaly score

For a given query color image, we calculate an anomaly score for each pixel. Importantly, herein, we propose a new anomaly score based on CIEDE2000 color difference which is designed in consideration of human visual characteristics. We expect that since CIEDE2000 reflects differences in colors as perceived by humans, it provides anomaly score that aligns with human visual inspection. Here we calculate CIEDE2000 color difference d_i from $\mathbf{I}'_c(x_i)$ and $\hat{\mathbf{I}}'_c(x_i)$. Then, the anomaly score used in this study is obtained simply by summing d_i for all i . We will briefly describe the concept of CIEDE2000 in the Appendix. For more details see [33].

Experiment

Dataset

To evaluate the performance of our anomaly detection method, we use a dataset which is publicly available through the PlantVillage project [1]. This dataset contains 54,306 images of healthy and diseased crop plants covering 14 crop species. The 14 crops are *Apple*, *Blueberry*, *Cherry*, *Corn*, *Grape*, *Orange*, *Peach*, *Bell Pepper*, *Potato*, *Raspberry*, *Soybean*, *Squash*, *Strawberry* and *Tomato*. There are three different versions of each image, namely *RGB color*, *Grayscale* and *Segmented*.

Examples of segmented images in the PlantVillage dataset are shown in Fig. 2 – (a) healthy leaves and (b) diseased leaves. For experiments, we used the potato plant segmented images which comprise of 152 healthy leaves and 1,000 early blight leaves. Early blight is caused by the fungus *Alternaria solani*. Symptoms appear on older leaves as small brown spots. As the disease progresses, it spreads throughout the leaf surface, eventually making it turn yellow and then wither.

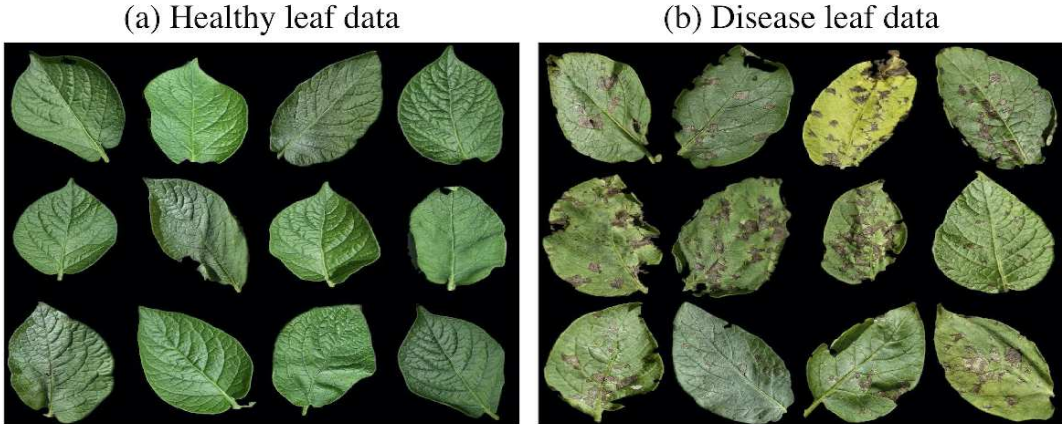


Fig 2. Examples of potato plant segmented images in the PlantVillage dataset. (a) Healthy leaf Data, (b) Diseased leaf Data.

We divided these images into training and test sets for pix2pix. The breakdown is shown in Table 1. Half of the healthy leaf images were allocated to the training set, and half to the test set. We randomly chose 100 diseased images for the test set. All images had a size of 256×256 pixels.

Table 1. Number of images used in the experiment.

Training data	Healthy leaf images	76
Test data	Healthy leaf images	76
	Diseased leaf images	100

Experimental Setup

Here we briefly describe the experimental setup for training GANs. The optimal problem described in Eq. 2 was solved by the Adam optimiser with a learning rate of 0.00015. Momentums were set to $\beta_1 = 0.5$, $\beta_2 = 0.999$. The discriminator has a PatchGAN architecture with a patch size of 64×64 . Training was terminated after 150 epochs. The hyperparameter for L_1 regularization was set to $\lambda = 10$.

For comparison, we use AnoGAN as a baseline method for evaluating detection performance. AnoGAN was also trained by the Adam optimizer. The learning rate was 0.0001. Momentums were set as per those of pix2pix. AnoGAN training was terminated after 2,000 epochs. The latent variable dimension in AnoGAN was set to 30. In calculations of anomaly scores, the weight coefficient for residual loss and the discrimination score are set to 0.9 and 0.1, respectively. In addition to this, we calculate simple color histogram similarity for measuring color differences aiming at highlighting a characteristic of CIEDE2000. The result of these comparisons will be discussed in Sec. .

The computational environment was as follows. We used Pytorch (version 1.3.0) code for pix2pix which is available at <https://github.com/phillipi/pix2pix>. We modified the Keras (version 2.2.4) code for AnoGAN which is available at <https://github.com/tkwoo/anogan-keras>. All computations were performed on a GeForce RTX 2028 Ti GPU based on a system running Python 3.6.9 and CUDA 10.0.130.

Visualization of color Differences at a Pixel Level

Fig. 3 shows examples of colorization results for test data. Results for healthy leaves of *Potatos* are shown in the upper column of Fig. 3 as *Healthy*. Two diseased leaf examples are shown in the middle and lower column of Fig. 3 as *Disease (1)* and *Disease (2)*. Original color images are shown in Fig. 3(a). Images in Fig. 3(b) are grayscale converted from the original color images. In Fig. 3(c), we present reconstructed color images by pix2pix. In Fig. 3(d), we show heat map visualizations on CIEDE2000 color difference between original color images and reconstructed color images. The warm color indicates a large color difference for each pixel.

By comparing Fig. 3(c) with Fig. 3(d), we can observe two important facts. First, healthy leaf images were successfully colorized throughout the images, at least in appearance. Second, symptomatic brown spots and yellow discoloration were not reconstructed. These results are aligned to our expectations, that is to say, since we trained pix2pix only with healthy-leaf images, the generator network could not reconstruct colors in symptomatic regions. Consequently, as seen from Fig. 3(d), symptomatic regions are highlighted by CIEDE2000 color differences. In contrast, there is no especially highlighted area on the healthy leaf image in Fig. 3(d).

To appreciate further characteristics of our approach, we compared our results with AnoGAN. In Fig. 3(e), we present reconstructed images by AnoGAN. These were translated from original color images by the generator network in AnoGAN, which is a deep convolutional auto-encoder network. Note that the generator network was trained by healthy leaf images as with pix2pix. In Fig. 3(f), we present heat map visualizations on residuals for each pixel between original color images and reconstructed images by AnoGAN. These heat maps were drawn in a same format as in Fig. 3(d).

As seen from Fig. 3(e), it is obvious that appearances of leaves were incompletely reconstructed by

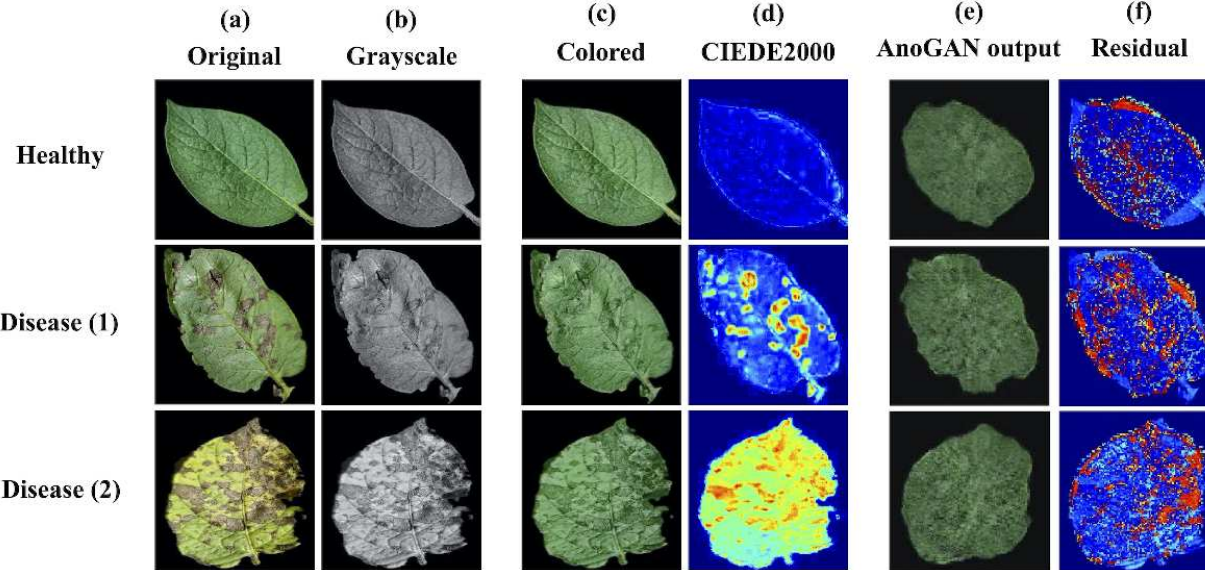


Fig 3. Examples of pixel-level disease visualization of plants. (a) Original color images. (b) Grayscale images converted from original color images. (c) Reconstructed color images by pix2pix. (d) CIEDE2000 color differences between original color images and reconstructed color images by pix2pix. (e) Reconstructed images by AnoGAN. (f) Residuals between original color images and reconstructed images by AnoGAN.

AnoGAN. As a natural consequence, pixel-level residuals shown in Fig. 3(f) were strongly affected by the incomplete reconstruction. Especially, we can see artificially highlighted regions around edges of leaves for both healthy and diseased cases. In contrast, as seen in *Disease(2)*, most symptomatic regions discolored in yellow were not highlighted in the heat map. These results suggest limitations of AnoGAN for visualizing symptomatic regions on plant leaves at a pixel level.

The incompleteness in reconstructing images by AnoGAN is most likely caused by a lack of training data. Accordingly, the reconstruction would be improved by adding healthy leaf images to the training data. However, in that case, it is also expected that the generator network in AnoGAN will fail to reconstruct diseased leaf images, and consequently it could generate substantive artifacts. It follows from these arguments that our approach provides a more efficient pixel-level visualization for interpreting anomalies in images in comparison with approaches based on AnoGAN. In addition, we note that the proposed method works well even though only 76 healthy-leaf images were used for training.

In Fig. 4, we additionally show examples of pixel-level disease visualization by the proposed method for *Grapes* and for *Strawberries*. As well as *Potatos*, we can see that symptomatic regions on these leaves are successfully highlighted. As we intended, the proposed method works well for detecting symptomatic regions of various plants.

Performance evaluation of image-level disease detection

Fig. 5 presents histograms for three anomaly scores. Fig. 5(a) pertains to the CIEDE2000 anomaly score, which corresponds to the proposed method. Fig. 5(b) represents the anomaly score calculated from color histogram similarity. Finally Fig. 5(c) concerns the anomaly score in AnoGAN. Red and blue indicate anomaly scores for healthy and diseased leaf images, respectively. From these figures, the CIEDE2000 anomaly score is intuitively more suitable for distinguishing healthy and diseased samples at an image level.

Next, we demonstrate the usability of the CIEDE2000 anomaly score in a more objective way. In Fig. 6, we show ROC curves for image-level disease detection based using three anomaly scores. The red line indicates the ROC curve based on the CIEDE2000 anomaly score. Similarly, ROC curves based on the anomaly scores calculated from color histogram similarity and AnoGAN are represented in blue and in green, respectively. The corresponding Areas Under ROC curves (AUC) are specified in parentheses

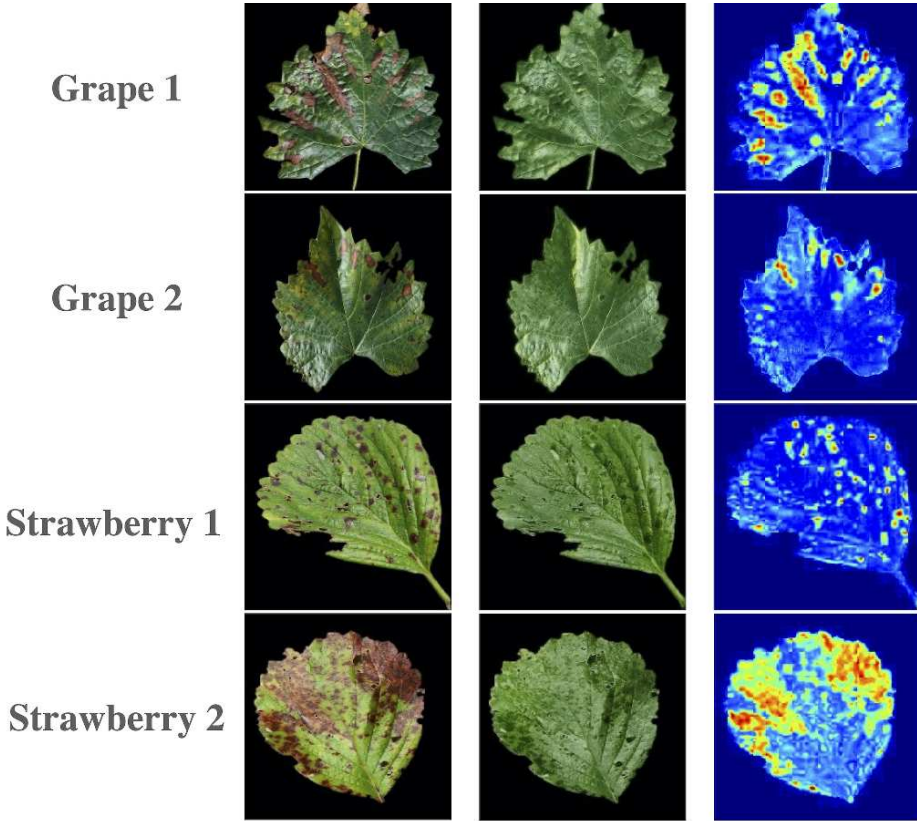


Fig 4. Other examples of pixel-level disease visualization for *Grapes* (shown in the first and the second column) and for *Strawberries* (shown in the third and the fourth column).
 (a) Original color images. (b) Reconstructed color images by pix2pix. (c) CIEDE2000 color differences.

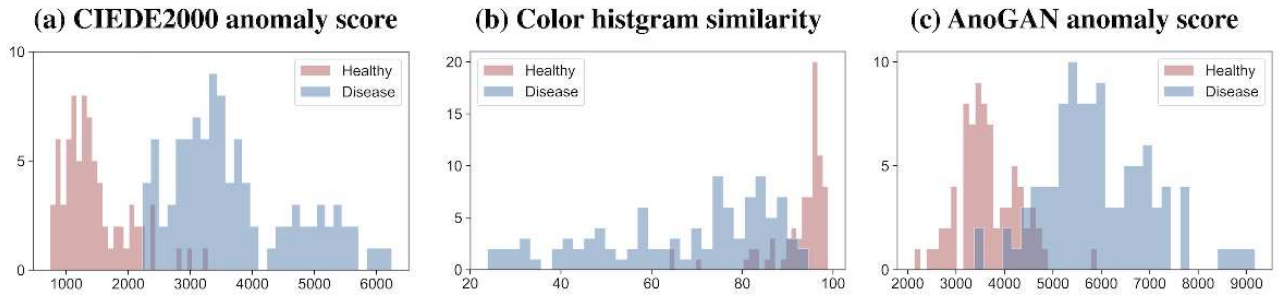


Fig 5. Histograms of three anomaly scores.

in the graph legend. Focusing on the outline of ROC curves, we can discern useful properties of the CIEDE2000 anomaly score. That is, it shows a high true positive rate with a low false positive rate,

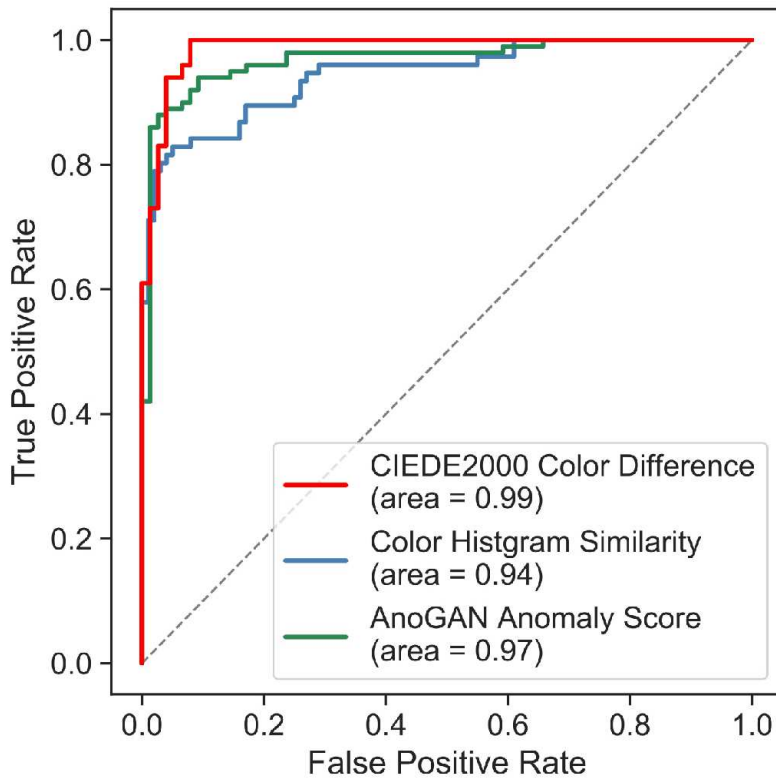


Fig 6. ROC curves based on three anomaly scores.

which is superior to two baseline anomaly scores.

Further, we demonstrate the statistical performance of our anomaly detection method for image-level disease detection. In Table 2, we present precision, recall and the F_1 -score. These indices were calculated based on the top-100 test images sorted in decreasing order with respect to anomaly scores. The best

Table 2. Performance comparison for image-level disease detection using the PlantVillage dataset.

Method	Precision	Recall	F_1 -Score	AUC
CIEDE2000 Anomaly Score	0.94	0.94	0.94	0.99
color Histogram Similarity	0.86	0.86	0.86	0.94
AnoGAN Anomaly Score	0.92	0.92	0.92	0.97

Table 3. Computation times for calculating anomaly scores.

	<i>Healthy</i>	<i>Diseased</i>
Our method (using pix2pix)	61.24 ± 17.21 ms	62.09 ± 18.33 ms
AnoGAN	$3,884 \pm 1,138$ ms	$4,574 \pm 1,538$ ms

performance in each index is emphasized by bold type. It is noteworthy that the performance of the CIEDE2000 anomaly score is superior to the two baseline anomaly scores through all indices.

Computational efficiency of anomaly score calculations

During detection, AnoGAN needs to determine the latent space location for a given query image based on iterative back propagation leading to the anomaly score [28] [31]. This determining process reduces the computational efficiency of AnoGAN. On the other hand, our approach does not require an iterative procedure during detection. In Table 3, we present mean computation times with standard deviations for calculating the CIEDE2000 anomaly score and the AnoGAN anomaly score. The values in the table are the times in milliseconds required to calculate the anomaly score for a given query image. These results suggest that our approach offers superior computational efficiency compared to AnoGAN; this is clearly an important consideration for practical real-time disease detection in plantations.

Conclusions

In this study, we proposed a novel approach relying on color reconstructability for detecting diseases in plant images. Similar to AnoGAN, our method detects anomalies of unseen data based on unsupervised training of a generator and discriminator by normal data. However, unlike AnoGAN, the present study focuses on anomalies in images dominantly appearing in color.

We compared the performance of our method with baseline methods including AnoGAN in terms of accuracy, interpretability and computational efficiency. Through experiments using the PlantVillage dataset, the proposed method was shown to exhibit superior performance compared with AnoGAN for image-level anomaly detection. Since the CIEDE2000 anomaly score is simple and aligns with human visual inspection, it provides an easily interpretable heat map visualization at the pixel level. In illustrative examples, symptomatic regions in leaves such as brown spots and yellow discoloration were efficiently highlighted. No serious artifacts were observed in either healthy leaf or diseased leaf images in contrast to the residual maps based on AnoGAN.

Since our approach does not require any iterative computation for calculating anomaly scores, the mean computation time was significantly improved compared to that of AnoGAN. The computational

efficiency of our approach could be practical for real-time image-based plant diseases detection. Future studies are warranted which explore practical automatic diagnosis systems for detecting diseases of plants on a massive global scale based on the idea of color reconfigurability.

Appendix

The CIEDE2000 color difference formula used to calculate anomaly scores is shown below. In this formula, the color space $L^*a^*b^*$ is used for calculation. This space is suitable for expressing colors based on human perception. The color difference is calculated based on three parameters: lightness difference ($\Delta L'$), chroma difference ($\Delta C'$) and hue difference ($\Delta H'$) weighted by the functions (S_L , S_C , S_H), parametric weighting factors (k_L , k_C , k_H) and a rotation term (R_T). All parametric weighting factors were set to $k_L = k_C = k_H = 1$.

The CIEDE2000 color difference between two points in the $L^*a^*b^*$ color space (L_1^*, a_1^*, b_1^*) and (L_2^*, a_2^*, b_2^*) is calculated by Eq. 3. The Python code used for implementing this CIEDE2000 color difference formula is available at <https://github.com/scikit-image/scikit-image>.

$$\Delta E_{00}(L_1^*, a_1^*, b_1^*, L_2^*, a_2^*, b_2^*) = \sqrt{\left(\frac{\Delta L'}{k_L S_L}\right)^2 + \left(\frac{\Delta C'}{k_C S_C}\right)^2 + \left(\frac{\Delta H'}{k_H S_H}\right)^2 + \left(R_T \left(\frac{\Delta C'}{k_C S_C}\right) \left(\frac{\Delta H'}{k_H S_H}\right)\right)^2} \quad (3)$$

Further details and a derivation of the CIEDE2000 color difference equation are provided in [33].

References

1. Hughes DP, Salathe M. An open access repository of images on plant health to enable the development of mobile disease diagnostics; 2016. Available from: [arXiv:1511.08060](https://arxiv.org/abs/1511.08060).
2. Mohanty SP, Hughes DP, Salathe M. Using deep learning for Image-Based plant disease detection. *Frontiers in Plant Science*. 2016;22.
3. Amara J, Bouaziz B, Algergawy A. A Deep Learning-based Approach for Banana Leaf Diseases Classification. In: *Lecture Notes in Informatics* 2017; 2017.
4. Ferentinos KP. Deep learning models for plant disease detection and diagnosis. *Computers and Electronics in Agriculture*. 2018;145:311–318.
5. Draško Radovanovic, Slobodan Dukanovic Image-Based Plant Disease Detection: A Comparison of Deep Learning and Classical Machine Learning Algorithms. In: 24th International Conference on Information Technology (IT); 2020.
6. Xiong L, Poczos B, Schneider JG. Group anomaly detection using flexible genre models. In: *NIPS* 2011; 2011. p. 1071–1079.
7. Zimek A, Schubert E, Kriegel H. A survey on unsupervised outlier detection in high dimensional numerical data. *Statistical Analysis and Data Mining*. 2012;5(5).
8. Chen Y, Zhou X, Huang TS. One-Class SVM for leaning in image retrieval. In: *Proceedings IEEE International Conference on Image Processing* 2001; 2001.

9. Chalapathy R, Menon AK. Robust, deep and inductive anomaly detection. In: Proceedings of ECML PKDD 2017; 2017.
10. Patterson J, Gibson A. Deep Learning: A Practitioner's Approach. O'Reilly Media, Inc.; 2017.
11. Tuor A, Kaplan S, Hutchinson B, Nichols N, Robinson S. Deep learning for unsupervised insider threat detection in structured cybersecurity data streams. In: Workshops at the Thirty-First AAAI Conference on Artificial Intelligence; 2017.
12. Sutskever I, Hinton G, Taylor G. The recurrent temporal restricted Boltzmann machine. In: Advances in Neural Information Processing Systems 21 (NIPS 2008); 2008. p. 1601–1608.
13. Vincent P, Larochelle H, Bengio Y, Manzagol PA. Extracting and composing robust features with denoising autoencoders. In: Proceedings of the 25th international conference on Machine learning; 2008. p. 1096–1103.
14. Rodriguez P, Wiles J, Elman JL. A recurrent neural network that learns to count. Connection Science. 1999;11(1):5–40.
15. Lample G, Ballesteros M, Subramanian S, Kawakami K, Dyer C. Neural architectures for named entity recognition. In: Proceedings of the 2016 Conference of the North American Chapter of the Association for Computational Linguistics: Human Language Technologies. San Diego, California: Association for Computational Linguistics; 2016. p. 260–270. Available from: <https://www.aclweb.org/anthology/N16-1030>.
16. Edmunds R, Feinstein E. Deep semi-supervised embeddings for dynamic targeted anomaly detection; 2017.
17. Racah E, Beckham C, Maharaj T, Kahou SE, Prabhat, Pal C. ExtremeWeather: A large-scale climate dataset for semi-supervised detection, localization, and understanding of extreme weather events. In: Advances in Neural Information Processing Systems; 2017. p. 3402–3413.
18. Perera P, Patel VM. Learning Deep Features for One-Class Classification. IEEE Transactions on Image Processing. 2019;28(11):5450–5463.
19. Chalapathy R. Generative Adversarial Networks; 2019. Available from: [arXiv:1901.03407](https://arxiv.org/abs/1901.03407).
20. Goodfellow IJ, Pouget-Abadie J, Mirza M, Xu B, Warde-Farley D, Ozair S, et al.. Deep learning for anomaly detection: A Survey; 2014. Available from: [arXiv:1406.2661](https://arxiv.org/abs/1406.2661).
21. Radford A, Metz L, Chintala S. Unsupervised representation learning with deep convolutional generative adversarial networks. In: ICLR2016; 2016.
22. Chen X, Duan Y, Houthooft R, Schulman J, Sutskever I, Abbeel P. InfoGAN: Interpretable Representation Learning by Information Maximizing Generative Adversarial Nets. In: NIPS2016; 2016.
23. Salimans T, Goodfellow I, Zaremba W, Cheung V, Radford A, Chen X. Improved techniques for training GANs; 2016. Available from: [arXiv:1606.03498](https://arxiv.org/abs/1606.03498).
24. Gulrajani I, Ahmed F, Arjovsky M, Dumoulin V, Courville A. Improved training of Wasserstein GANs. In: NIPS2017; 2017.
25. Mao X, Li Q, Xie H, Lau RYK, Wang Z, Smolley SP. Least squares Generative Adversarial Networks. In: 2017 IEEE International Conference on Computer Vision (ICCV); 2017.

26. Isola P, Zhu JY, Zhou T, Efros AA. Image-to-Image translation with conditional adversarial networks. In: 2017 IEEE Conference on Computer Vision and Pattern Recognition (CVPR); 2017.
27. Donahue J, Krahenbuhl P, Darrell T. Adversarial feature learning. In: The International Conference on Learning Representations (ICLR); 2017.
28. Schlegl T, Seeböck P, Waldstein SM, Schmidt-Erfurth U, Langs G. Unsupervised anomaly detection with Generative Adversarial Networks to guide marker discovery. In: International Conference on Information Processing in Medical Imaging; 2017. p. 146–157.
29. Zenati H, Foo CS, Lecouat B, Manek G, Chandrasekhar VR. Efficient GAN-Based anomaly detection. In: 6th International Conference on Learning Representations (ICLR2018); 2018.
30. Akcay S, Atapour-Abarghouei A, Breckon TP. GANomaly: semi-supervised anomaly detection via adversarial training; 2018. Available from: [arXiv:1805.06725](https://arxiv.org/abs/1805.06725).
31. Schlegl T, Seeböck P, Waldstein SM, Langs G, Schmidt-Erfurth U. f-AnoGAN: Fast unsupervised anomaly detection with generativeadversarial networks. Medical Image Analysis. 2019;54:30–44.
32. Riley MB, Williamson MR, Maloy O. Plant Disease Diagnosis; 2002. Available from: <https://www.apsnet.org/edcenter/disimpactmngmnt/casestudies/Pages/PlantDiseaseDiagnosis.aspx>.
33. Sharma G, Wu W, Dalal EN. The CIEDE2000 color-difference formula: implementation notes, supplementary test data, and mathematical observations. Color Research and Application. 2005;30(1).